Optimization of $In_{0.20}Ga_{0.80}N$/GaN-Based TCAD Design for Intermediate band Solar cell: Temperature impact

Salaheddine Amezzoug[(1,)], Haddou El Ghazi[(1,2,*)], Abderrazzak Bouziane[(1)], Walid Belaid[(2,3,*)], Ahmed Sali[(4)]*

[(1)] *SCDRE Group, CCPS laboratory, ENSAM, Hassan II University, Casablanca, Morocco*
[(2)] *School of Electronic and Electrical Engineering, University of Leeds, Leeds LS2 9JT, UK*
[(3)] *Laser Spectroscopy Group, Faculty of Sciences, Selçuk University, 42075 Konya, Turkey*
[(4)] *LPS, Faculty of Sciences, Sidi Mohamed Ben Abdellah University, Fes, Morocco*
[(*)] *Correspondence: salaheddineamezzoug@gmail.com; elghazi.haddou@ensam-casa.ma; w.belaid@leeds.ac.uk.*

Abstract

Intermediate-band solar cells offer the potential to surpass the Shockley-Queisser efficiency limit in single-junction architectures, though optimal material systems and device configurations remain subjects of active investigation. This study presents comprehensive two-dimensional device-level simulations utilizing Silvaco Atlas TCAD software to analyze p-i-n $In_{0.20}Ga_{0.80}N$/Gan solar cell performance with an intermediate band generated by $In_{0.20}Ga_{0.80}N$ quantum dot arrays embedded within the intrinsic region. This study presents the modeling and simulation of a quantum dot solar cell based on the **$In_{0,20}Ga_{0,80}N$/GaN** material system. The investigation encompasses comprehensive analysis of key photovoltaic parameters including short-circuit current density Jsc, open-circuit voltage Voc, fill factor FF and power conversion efficiency of the **$In_{0,20}Ga_{0,80}N$/GaN** quantum dot solar cell QDSC under different temperatures employing AM1.5 solar spectrum illumination at one-sun intensity. Temperature-dependent characterization reveals systematic performance degradation with increasing operating temperature, with conversion efficiency decreasing from 47,38% at 295 K to 45,85% at 335 K, representing a relative reduction of 3.23% over this temperature range.

Keywords: intermediate-band Solar cells IBSC; InGaN quantum dots; III-N wide-bandgap semiconductors; p-i-n junction; TCAD device simulation; photovoltaic device modelling.

Introduction

Intermediate band solar cell performance has been enhanced through the incorporation of low-dimensional nanostructures such as quantum wells (QWs), quantum wires (QWires), and quantum dots (QDs). Under concentrated illumination, quantum dot solar cells (QDSC) have demonstrated maximum theoretical conversion efficiencies approaching 63.1%[1][2]. The exceptional optoelectronic properties of QDs originate from their zero-dimensional (0D) electronic confinement, generating significant fundamental and technological interest [3]. In these nanostructures, charge carriers occupy discrete energy levels due to three-dimensional spatial confinement[4]. QD formation involves embedding small-bandgap material inclusions within a larger-bandgap host matrix. For electronic state quantization to occur, the nanostructure dimensions must be comparable to or smaller than the de Broglie wavelength of charge carriers, typically several tens of nanometers[5]. Performance optimization of quantum dot solar cells depends critically on material selection and processing control. While silicon-based technologies dominate microelectronics applications, enhancing their electronic and transport properties remains challenging. Consequently, research efforts have increasingly focused on III-V compound

semiconductors, which offer direct bandgap characteristics where valence band maxima and conduction band minima coincide at the same k-point in the Brillouin zone, enabling superior optical absorption and emission efficiency[6][7]. The InGaN material system exhibits exceptional properties for low-dimensional semiconductor device applications. $In_xGa_{1-x}N$ alloys have been successfully fabricated with varying indium compositions, yielding promising experimental results. The superior characteristics of $In_xGa_{1-x}N$ make it an attractive material for quantum dot solar cell architectures, meriting comprehensive theoretical investigation. InGaN-based solar cells offer substantial potential for achieving ultra-high conversion efficiencies in both terrestrial and space applications due to several key material advantages. The alloy system spans a wide bandgap range from 0.7 eV (InN) to 3.42 eV (GaN)[8][9], enabling bandgap engineering through indium composition control to optimize spectral coverage across the solar spectrum. Additional favorable properties include high optical absorption coefficients ($>10^5$ cm^{-1}), excellent radiation hardness for space environments, and intrinsic polarization and piezoelectric effects that can enhance carrier separation. These attributes collectively position $In_xGa_{1-x}N$/GaN quantum dot heterostructures as promising systems for next-generation high-efficiency photovoltaic devices[10][11].

Quantum-confined heterostructures have emerged as a viable approach for enhancing photovoltaic conversion efficiency beyond the Shockley-Queisser limit[4][12]. Multiple quantum dots (MQDs) and superlattice (SL) configurations integrated within the intrinsic region of p-i-n junction devices enable sub-bandgap photon absorption while maintaining charge separation through the built-in electric field. These structures exploit the quantum size effect to tune the effective bandgap and extend the spectral response of wide-bandgap host semiconductors. Multiple quantum dot (QD) implementations in photovoltaic devices present competing mechanisms that determine overall device performance. Sub-bandgap photon absorption by quantum-confined states increases the short-circuit current density (J_{sc}) through enhanced carrier generation[13]. However, spatial localization of carriers within quantum wells introduces additional recombination centers, resulting in reduced open-circuit voltage (V_{oc}) and fill factor degradation. The QDSC architecture consists of a p-i-n junction with periodic insertion of narrow-bandgap quantum wells within the intrinsic layer. These quantum-confined regions, create a band alignment that spatially separates electrons and holes. This study presents a comprehensive theoretical analysis of $In_{0,20}Ga_{0,80}N$/GaN IB-QDSC using drift-diffusion modeling coupled with quantum mechanical calculations using Silvaco Atlas TCAD device simulator. The investigation examines the parametric dependence of device characteristics on temperature-dependent profile to establish design criteria for optimized photovoltaic performance.

NUMERICAL MODELING OF p-i-n MULTIPLE QUANTUM DOT SOLAR CELLS USING ATLAS TCAD

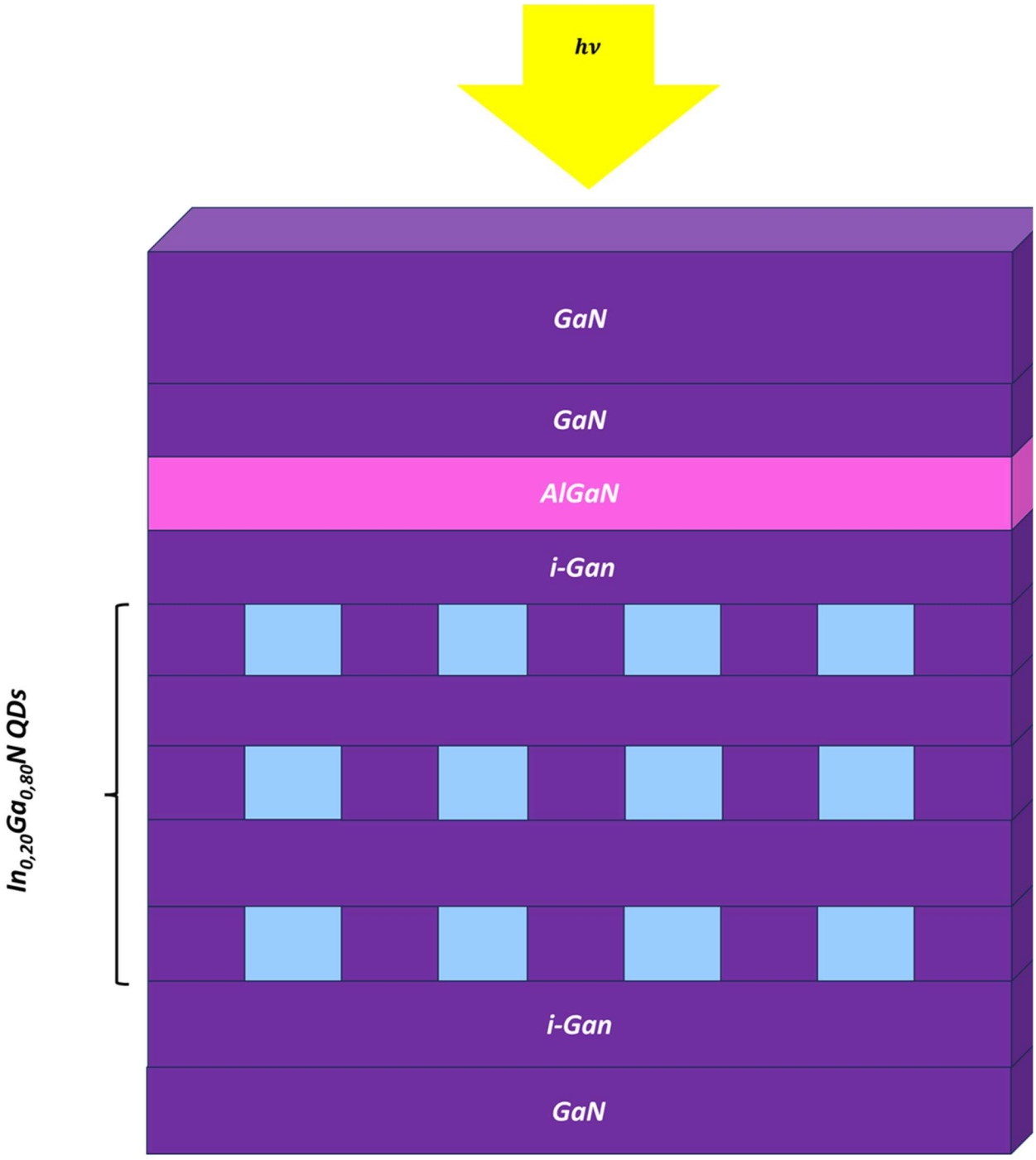

Fig.1. The schematic diagram of the present $In_{0.20}Ga_{0.80}N/GaN$ Quantum Dots Solar Cell with three layers of quantum dots embedded in the intrinsic region is shown in the figure are sandwiched between GaN p- and n-type layers. Al0.1Ga0.90N which called Electron Blocking Layer (EBL) provides sufficient potential barrier height to confine electrons in the conduction band.

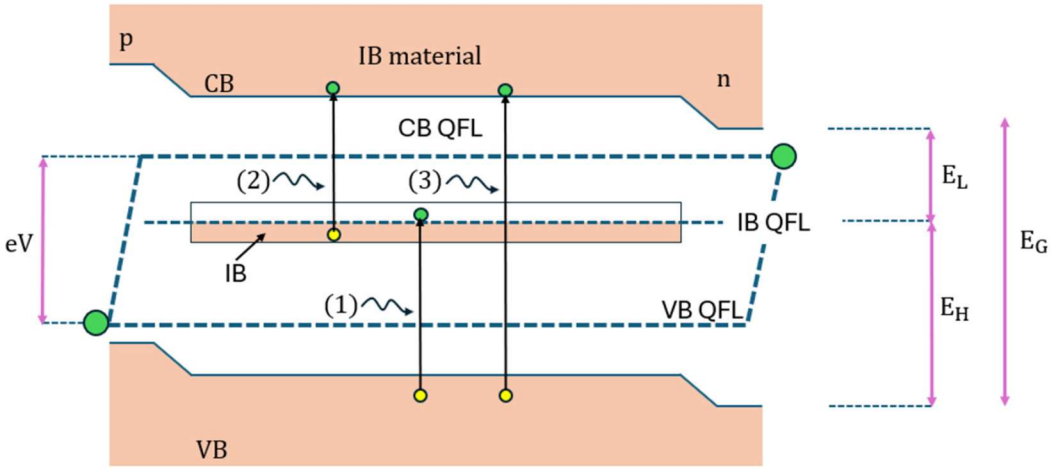

*Fig. 2: Band diagram of a **p-i-n solar cell** featuring an **intermediate band (IB)** within the material's bandgap (E_g). The IB facilitates a two-step absorption of two sub-bandgap photons to generate a single electron-hole pair.*
*The diagram shows a **two-photon absorption** mechanism in an intermediate band solar cell. **Transition (1)** depicts the excitation of an electron from the valence band (VB) to the IB. **Transition (2)** shows the subsequent promotion of the electron from the IB to the conduction band (CB). This two-step process achieves the same electron-hole pair generation as a single, high-energy **Transition (3)**. By capturing lower-energy photons, this mechanism increases the short-circuit current (J_{SC}). The open-circuit voltage (V_{OC}), however, is ideally preserved because it is dictated by the energy difference between the quasi-Fermi levels of the conduction band and valence band[11].*

The computational analysis of multiple quantum dot solar cells (MQDSCs) employs the established p-i-n junction configuration as the fundamental device architecture. Within the ATLAS simulation environment, quantum dot ensembles are positioned throughout the intrinsic layer to form a nanostructured absorber region. The incorporation of $In_{0,20}Ga_{0,80}N$/GaN quantum dots establish a complex energy landscape characterized by discrete energy levels and modified density of states, effectively creating a multi-bandgap absorption system. This quantum confinement architecture generates localized potential minima that trap charge carriers while simultaneously enabling controlled carrier release through thermal activation and field-enhanced tunneling processes. The presence of the space charge region electric field facilitates efficient carrier extraction by providing the necessary driving force for charge transport from quantum-confined states to the respective collection electrodes. This field-assisted mechanism enhances the probability of carrier collection while suppressing recombination losses through reduced carrier residence time within the active region.

The fitted empirical band gap with compositions dependent band bowing:

$$E_g(In_xGa_{1-x}N) = x.E_g^{InN} + (1-x).E_g^{GaN} - b.x.(1-x) \quad (1)$$

Where, the bowing parameter depends on the composition b(x) is given by:

$$b_x = \frac{9.5}{1+10.4x} \quad (2)$$

Results and discussion

All simulations are conducted under standard test conditions employing AM1.5 solar spectrum illumination at one-sun intensity (1000 W/m²). The quantum dot solar cell $In_{0,20}Ga_{0,80}N/GaN$ architecture incorporates three discrete quantum dot layers uniformly distributed within the intrinsic region to maximize photon absorption while maintaining carrier collection efficiency. Temperature-dependent device characteristics are investigated across the operational range to elucidate thermal effects on photovoltaic performance parameters. Temperature significantly influences both optical absorption, optical generation processes and carrier transport mechanisms within semiconductor devices through multiple physical pathways. The fundamental relationship between temperature and material properties manifests primarily through bandgap modulation, which directly impacts absorption coefficient, carrier generation rates, and recombination dynamics. Bandgap energy temperature dependence exhibits material-specific behavior governed by electron-phonon interactions and thermal lattice expansion. The temperature coefficient of the bandgap energy varies considerably among different semiconductor materials due to variations in crystal structure, bond strength, and phonon coupling mechanisms. This temperature-induced bandgap energy variation is accurately described by the Varshni empirical relationship:

$$E_g = E_g(0) - \frac{\alpha T^2}{T + \beta}(3) \quad [10]$$

Where T is the junction temperature, $E_g(0)$ is the band gap energy at T = 0K, α and β are material-specific empirical constants characteristic of a given material.

Figure 3 illustrates the power-voltage (P-V) characteristics of the p-i-n $In_{0.20}Ga_{0.80}N/GaN$ quantum dot solar cell as a function of operating temperature. The results demonstrate a systematic reduction in maximum power output with increasing temperature, with conversion efficiency decreasing from 47.38% at 295 K to 45.85% at 335 K, corresponding to a temperature coefficient of approximately -0.038%/K over the investigated thermal range.

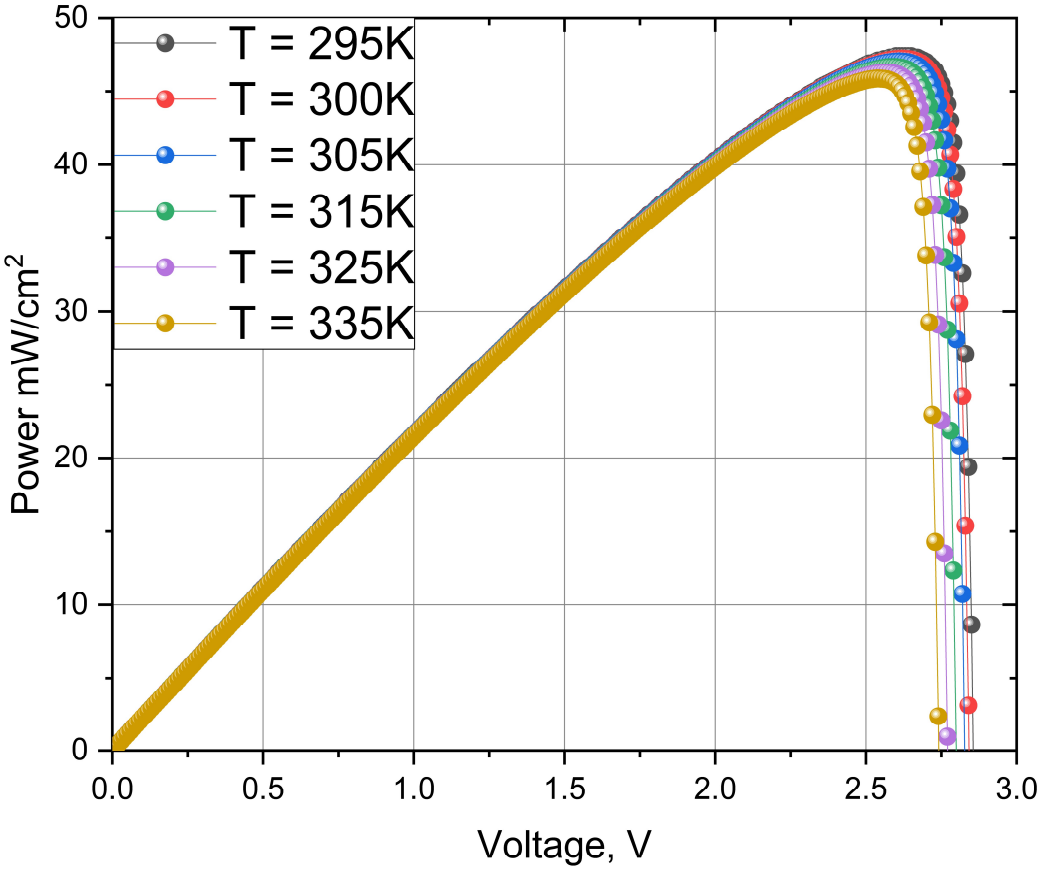

Fig. 3: Power output as a function of voltage for the p-i-n quantum dot solar cell under varying temperature conditions (295 K to 335 K).

Figure 4 illustrates the current density-voltage (J-V) characteristics of the $In_{0.20}Ga_{0.80}N$/GaN quantum dot solar cell under varying temperature conditions. As shown in Figures 4 and 5, both open-circuit voltage V_{oc} and short-circuit current density J_{sc} exhibit systematic degradation with increasing temperature. Over the temperature range from 295 K to 335 K, J_{sc} decreases marginally from 22.62 to 22.51 mA/cm², representing a relative reduction of 0.49%. In contrast, V_{oc} demonstrates more pronounced thermal sensitivity, declining from 2.85 V to 2.74 V (3.86% reduction) over the same temperature interval. The near-linear temperature dependence of both parameters is consistent with thermally-induced bandgap narrowing and enhanced carrier recombination mechanisms.

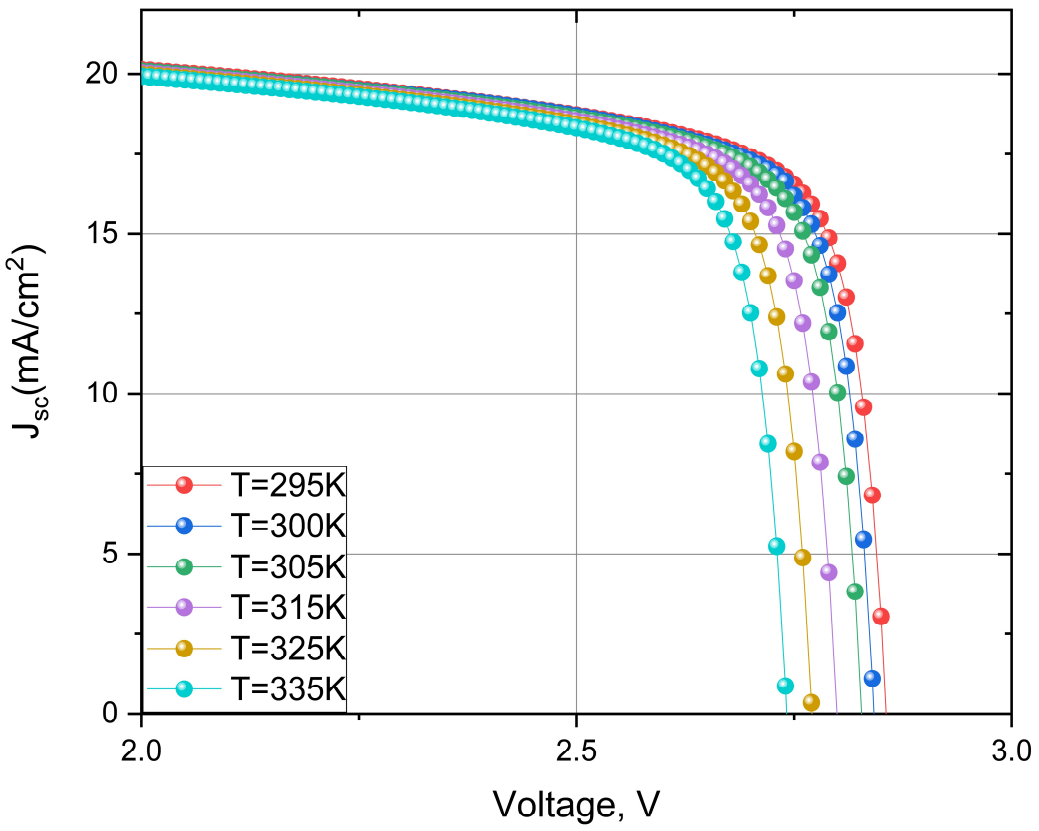

Fig. 4: Current density-voltage (J-V) characteristics of the p-i-n quantum dot solar cell as a function of temperature (295–335 K).

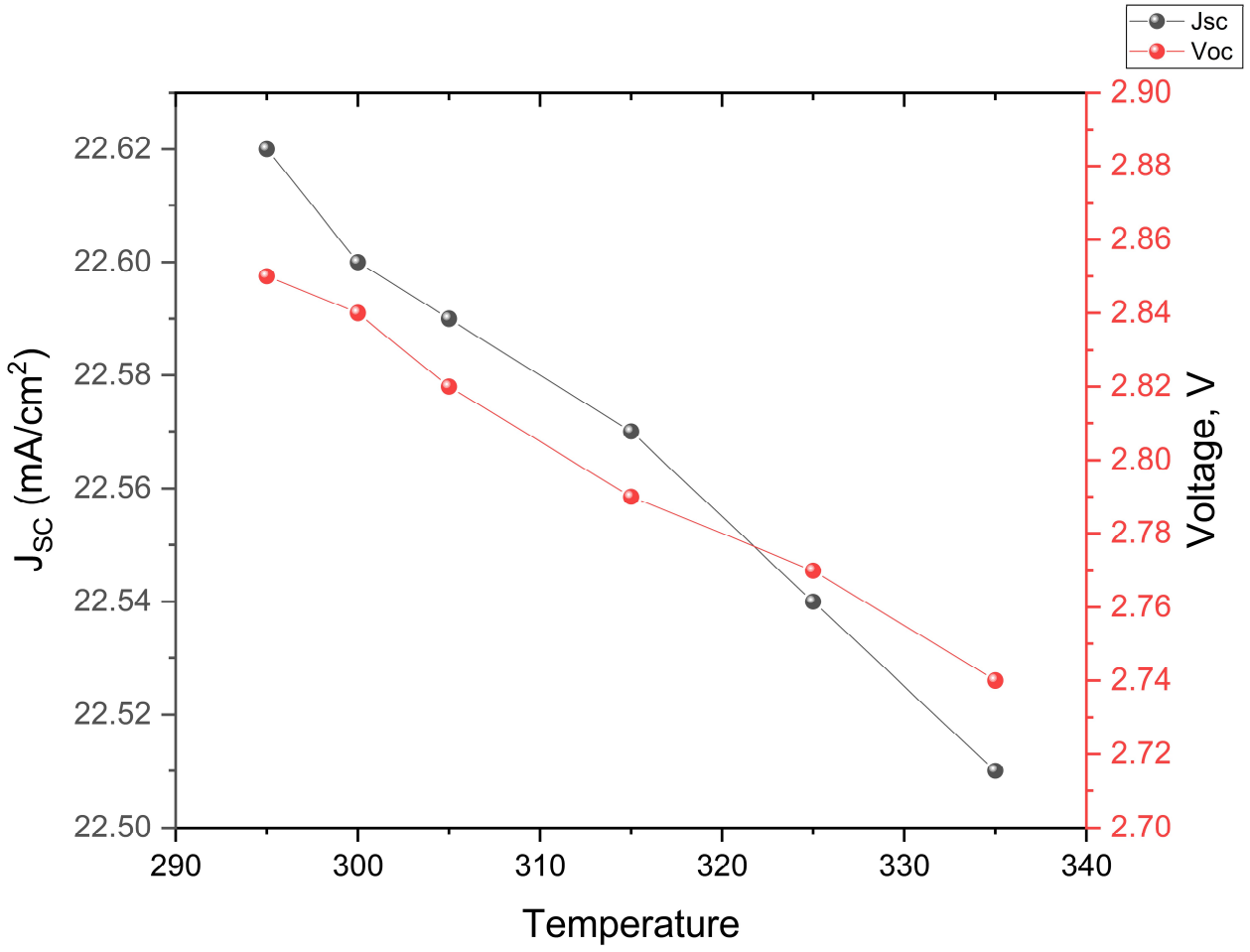

Fig. 5: Temperature dependence of short-circuit current density (J_sc) and open-circuit voltage (V_oc) for the p-i-n quantum dot solar cell.

The overall power conversion efficiency exhibits systematic degradation with increasing temperature, declining from 47.38% at 295 K to 45.85% at 335 K, representing a 3.23% relative reduction. This corresponds to a temperature coefficient of approximately -0.038%/K over the investigated thermal range.

Interestingly, the fill factor demonstrates opposite behavior, increasing from 73.36% to 74.32% 1.31% improvement with rising temperature. This enhancement is attributed to improved carrier mobility and reduced series resistance at elevated temperatures. However, this beneficial effect is insufficient to compensate for the concurrent degradation in both J_{SC} and V_{OC}. Consequently, the net result remains an overall efficiency decline, with voltage losses being the dominant factor limiting high-temperature performance.

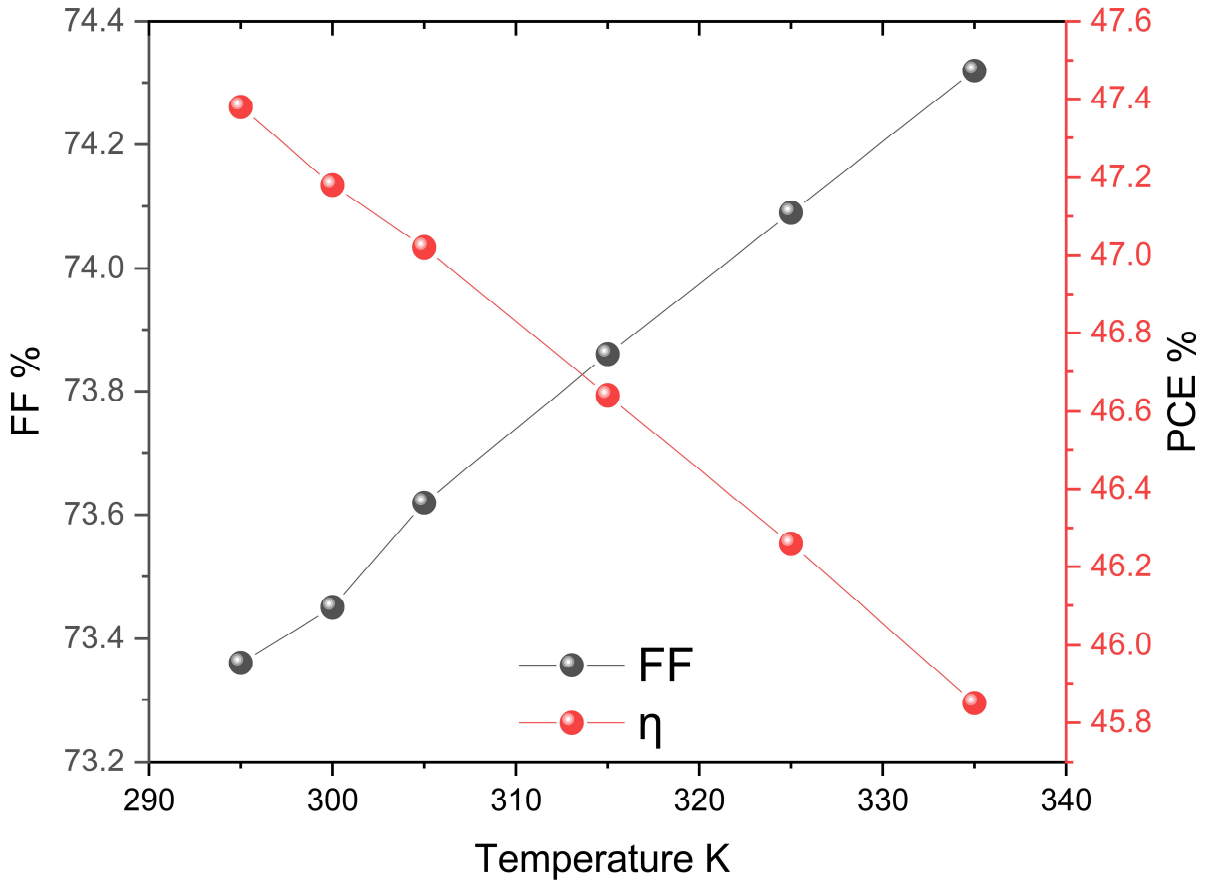

Fig. 6: Temperature dependence of power conversion efficiency (η) and fill factor (FF) for the p-i-n quantum dot solar cell.

Conclusion

This study presents comprehensive numerical simulations of an $In_{0.20}Ga_{0.80}N$/GaN quantum dot solar cell using Silvaco Atlas TCAD software to investigate the impact of temperature variation on key photovoltaic performance characteristics. A complete device structure was implemented incorporating optical constants for the InGaN/GaN material system and employing appropriate physical models for carrier transport and generation-recombination processes.

All simulations were conducted under standard AM1.5G solar spectrum at one-sun illumination intensity. The results demonstrate that temperature variation significantly affects the J-V characteristics, with both J_{sc} and V_{oc} exhibiting systematic degradation with increasing temperature. Short-circuit current density decreased marginally from 22.62 mA/cm² at 295 K to 22.51 mA/cm² at 335 K, representing a relative reduction of 0.49%. In contrast, open-circuit voltage showed more pronounced thermal sensitivity, decreasing from 2.85 V at 295 K to 2.74 V at 335 K (3.86% reduction). Consequently, power conversion efficiency declined from 47.38% to 45.85%, corresponding to a temperature coefficient of approximately -0.038%/K over the investigated thermal range.

Appendix

Table 1. Materials parameters at 300 K

Parameters at T = 300 K	*GaN*	*$In_{0,20}Ga_{0,80}N$*	*$Al_{0,10}Ga_{0,90}N$*
$E_g(eV)$	*3.42*	*2.42*	*1.21*
$\varepsilon(F/cm)$	*8.90*	*10.18*	*8.86*
$\chi(eV)$	*4.09*	*4.39*	*4.5*
$MUN(cm^2/V.s)$	*1000*	*1104.8*	*690*
$MUP(cm^2/V.s)$	*170*	*171.3*	*11.4*
$\tau_n(ns)$	*1*	*1*	*1*
$\tau_n(ns)$	*1*	*1*	*1*

the following sections describe the physical models used in this simulation:
Shockley-Read-Hall (SRH) recombination with concentration-dependent lifetimes was used to calculate carrier recombination rates according to:

$$R_{SRH} = \frac{pn - n^2}{\tau_n\left[n + n_i exp\left(\frac{ETRAP}{KT_L}\right)\right] + \tau_p\left[p + p_i exp\left(\frac{-ET}{KT_L}\right)\right]} \quad (4)$$

In this equation, ETRAP is the difference between the trap energy level and the intrinsic Fermi level..
Quantum confinement effects were treated using the self-consistent Schrödinger-Poisson model. The one-dimensional equations for electrons and holes are:

$$\frac{-\hbar^2}{2}\frac{\partial}{\partial x}\left(\frac{1}{m_e^*}\frac{\partial \Psi_i}{\partial x}\right) + E_c(x)\Psi_i = E_i\Psi_i \quad (5)$$

$$\frac{-\hbar^2}{2}\frac{\partial}{\partial x}\left(\frac{1}{m_h^*}\frac{\partial \Psi_i}{\partial x}\right) - E_v(x)\Psi_i = E_i\Psi_i \quad (6)$$

Where Ec and Ev are the conduction band and valence band edge respectively, m_e^* and m_h^* are the electron and hole effective masse respectively. Ψi and Ei are the wavefunction and energy level of sub-band.

References

[1] F. Benyettou, A. Aissat, and J. P. Vilcot, “Modeling and simulation of InAsP/GaAs quantum well solar cell,” in *Proceedings of 2015 IEEE International Renewable and Sustainable Energy Conference, IRSEC 2015*, Institute of Electrical and Electronics Engineers Inc., Apr. 2016. doi: 10.1109/IRSEC.2015.7455116.

[2] I. M. Ahmed, O. I. Alsaif, and Q. T. Algwari, “The Effect of Quantum Dots on the Performance of the Solar Cell,” *Iraqi Journal for Electrical and Electronic Engineering*, vol. 20, no. 2, pp. 236–242, Dec. 2024, doi: 10.37917/ijeee.20.2.20.

[3] F. Benyettou, A. Aissat, M. A. Benamar, and J. P. Vilcot, “Modeling and Simulation of GaSb/GaAs Quantum Dot for Solar Cell,” in *Energy Procedia*, Elsevier Ltd, 2015, pp. 139–147. doi: 10.1016/j.egypro.2015.07.535.

[4] M. Iqbal Chowdhury, S. Shafkat Nawaz, F. Noor Nowrin Haque, and M. Iqbal Bahar Chowdhury, “Silvaco TCAD Implementation of GaAs/GaSb Quantum Dot Solar Cell”, doi: 10.5281/zenodo.7502877.

[5] B. Fethi, A. Aissat, F. Benyettou, and J. P. Vilcot, “Modélisation et simulation des cellules solaires à puits quantique à base de SiGe/Si,” 2015. [Online]. Available: https://www.researchgate.net/publication/304011241

[6] A. Bakiri, B. Zaidi, K. Aouadj, S. Gagui, and M. S. Ullah, “Design and simulation of inxga1xn based solar cells,” *Acta Phys Pol A*, vol. 139, no. 1, pp. 46–50, Jan. 2021, doi: 10.12693/APhysPolA.139.46.

[7] A. Aissat, H. Arbouz, S. Nacer, F. Benyettou, and J. P. Vilcot, “Efficiency optimization of the structure pin-InGaN/GaN and quantum well-InGaN for solar cells,” *Int J Hydrogen Energy*, vol. 41, no. 45, pp. 20867–20873, Dec. 2016, doi: 10.1016/j.ijhydene.2016.06.028.

[8] B. Deepak Kumar Mangal *et al.*, “TCAD Based Simulation and Performance Optimization of InxGa(1-X)N based Solar Cell,” 2019.

[9] M. Benaicha, L. Dehimi, and N. Sengouga, “Simulation of double junction In0:46Ga0:54N/Si tandem solar cell,” *Journal of Semiconductors*, vol. 38, no. 4, 2017, doi: 10.1088/1674-4926/38/4/044002.

[10] A. Aissat, F. Benyettou, and J. P. Vilcot, “Modeling and simulation of InGaN/GaN quantum dots solar cell,” in *AIP Conference Proceedings*, American Institute of Physics Inc., Jul. 2016. doi: 10.1063/1.4959410.

[11] S. Amezzoug, H. El Ghazi, and W. Belaid, “TCAD Design and Optimization of In0.20Ga0.80N/In0.35Ga0.65N Quantum-Dot Intermediate-Band Solar Cells,” *Crystals (Basel)*, vol. 15, no. 8, p. 693, Jul. 2025, doi: 10.3390/cryst15080693.

[12] I. Bahar Chowdhury, M. Iqbal Chowdhury, M. Johirul Islam, and S. Nura Nabiah, “Silvaco TCAD Implementation of All-InGaN Based Quantum Well Solar Cell,” 2024, doi: 10.5281/zenodo.12703123.

[13] A. Aissat, M. Boubakeur, F. Benyettou, and J. P. Vilcot, “Optimization of Structure InAsx Sb1- xl GaAs Quantum Dot Solar Cell,” in *Proceedings of 2017 International Renewable and Sustainable Energy Conference, IRSEC 2017*, Institute of Electrical and Electronics Engineers Inc., Sep. 2018. doi: 10.1109/IRSEC.2017.8477379.